Magnetic Field Analysis and Thrust Verification of Solenoid Actuator Based on Subdomain Method

Mengkun Lu , Zhifang Yuan , Xianglie Yi *

Posted Date: 18 April 2024

doi: 10.20944/preprints202404.1258.v1

Keywords: Solenoid actuator; subdomain method; magnetic vector potential; push-pull electromagnet; movable iron-core

 doi:10.20944/preprints202404.1258.v1

Article

Magnetic Field Analysis and Thrust Verification of Solenoid Actuator Based on Subdomain Method

Mengkun Lu [1], Zhifang Yuan [2] and Xianglie Yi [2,*]

[1] School of Mechanical Engineering, Hubei Engineering University, Xiaogan 432000, China
[2] School of Electrical Engineering, Naval University of Engineering, Wuhan 430033, China
* Correspondence: yxljht@126.com;

Abstract: In view of the problem that the output thrust of solenoid actuator is affected by various factors and is difficult to calculate in actual working conditions, this paper proposes a semi-analytical model constructed by magnetic field subdomain method with internal and external boundary conditions in cylindrical coordinate system for calculation, and the general solution equations of magnetic vector potential for each subdomain are derived and solved by MATLAB. Taking a push-pull electromagnet as an example, the finite element simulation and experimental comparative analysis are carried out. The correctness and applicable conditions of the subdomain method are illustrated by comparing the gradient plot of magnetic vector potential, inductance curve and electromagnetic force. By calculating the output thrust after considering the core gravity, spring force and electromagnetic force, it is shown that this method has the advantage of computational flexibility compared with the finite element method, and it is easier to write special algorithms according to various working conditions to calculate the important parameters in engineering applications.

Keywords: Solenoid actuator; subdomain method; magnetic vector potential; push-pull electromagnet; movable iron-core

1. Introduction

Solenoid actuator is a cylindrical coil device with a movable iron-core inside [1]. Its working principle conforms to Ampere's law. When a current is passed through the coil in any direction, an electromagnetic (EM) field will be formed, and the iron-core will be magnetized by the magnetic field. According to the principle of minimum reluctance, the iron-core will be subjected to electromagnetic force (EMF) and move toward the center of the coil [2,3]. Solenoid actuator is a typical EM energy and mechanical energy conversion device, which can output straight line motion directly. In some scenarios that require short-distance linear motion control, solenoid actuators have unique advantages in terms of volume, quality, response speed and other performance compared to the combination of rotary motors with motion conversion devices [4]. Therefore, various mechanical devices developed based on the working principle of solenoid actuators emerge in an endless stream. In addition to the push-pull electromagnet, solenoid valves, relays, etc., there are also EM brakes, damping solenoids, EM suction solenoids, etc., which are widely used in the field of industrial automation.

Most of the solenoids in the civilian field will add a ferromagnetic material shell, which can effectively improve the magnetic permeability outside the coil, thereby improving the EMF of the iron-core and improving the efficiency [5]. However, the disadvantage is that it will generate EM heat, is not resistant to corrosion, and is not insulated. When the ferromagnetic shell is disturbed by the external magnetic field, it is easy to be misactivated [6], and resulting in accidents. For some special applications such as military, stability and safety are more important than other characteristics, the shell is often made of non-conductive, non-magnetic, high-temperature-resistant, corrosion-resistant polymer materials that are integrally injection molded to achieve full closure.

As a basic application technology, solenoid actuator has always been the key research direction of domestic and foreign researchers. In recent years, with the development of industrial technology

 doi:10.20944/preprints202404.1258.v1

and more and more attention to the application of electric energy, some new application methods of solenoid actuators have appeared one after another. Which including EM riveting machines for large-scale rivet riveting for the skin shell plate of large aircraft [7]; A linear piston pump was analyzed in [8], which is characterized by the fact that the EMF is directly applied to the piston to output hydraulic power instead of being converted from rotational power, which is more suitable for a compact packaging environment; A space docking scheme for small satellites was introduced in [9]; A modular satellite assembly scheme is dis-closed in [10].

However, due to the movement of the iron-core in solenoid actuator, there is a nonlinear relationship between EM data such as EMF, core position, and exciting current, it is difficult to calculate the magnetic field by analytical method. In the research of magnetic field calculation of solenoid, the magnetic without iron-core is easy to calculate according to Biot-Savart's law [11,12], while the algorithm theory of solenoid with movable iron-core is complicated and immature, there are few theoretical results. Currently available methods including semi-analytical calculation method and finite element method (FEM) [12], where semi-analytical method includes lumped parameter magnetic circuit model method and magnetic field subdomain method based on Poisson equation and Laplace equation [13]. The FEM has the problems of slow calculation speed and poor flexibility [14]; The lumped parameter magnetic circuit model method mainly calculates the average value of the magnetic field, rather than the detailed distribution of a region [13], and the calculation accuracy is limited; The magnetic field subdomain method has high accuracy and calculation speed under the condition of high permeability and non-magnetic saturation of the core. In [14–17], the process of solving magnetic induction, inductance and EMF of solenoid with iron-core by subdomain method is described theoretically.

Compared with FEM, semi-analytical calculation method has the advantages of fast calculation speed and programmable, and can complete many calculation tasks that the FEM cannot handle. At present, the method of calculating the magnetic field of solenoid actuator by subdomain method has a preliminary theoretical basis, but it lacks experimental verification and is not related to the engineering application products, and the feasibility and engineering value are not shown. In this study, a push-pull electromagnet without a ferromagnetic shell is used as an example to analyze the magnetic field subdomain method, and the magnetic vector potential equations with special functions such as Bessel is deduced, and the numerical solution is calculated by MATLAB programming. The finite element simulation results and experimental results show the feasibility of the method, and the engineering application value of the method is demonstrated through the calculation of the output thrust of the iron-core.

2. Magnetic Field Subdomain Model

3.1. Magnetic Vector Equation in Subdomain

The push-pull electromagnet is a common solenoid actuator, and its mechanical structure is mainly composed of an excitation coil, a movable iron-core and a spring. When there is no current in the coil, the iron-core will form an extended state under the action of the spring. When a current is applied to the coil in any direction, the iron-ore will move to the center of the coil, thereby forming a retracted state of the electromagnet. Figure 1 shows the structure diagram of the push-pull electromagnet without ferromagnetic shell.

Preprints.org (www.preprints.org) | NOT PEER-REVIEWED | Posted: 18 April 2024 doi:10.20944/preprints202404.1258.v1

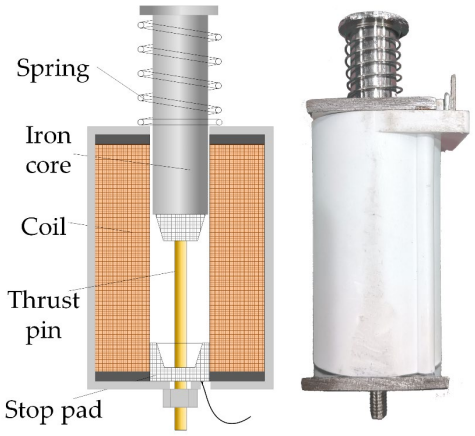

Figure 1. Structure diagram of a push-pull electromagnet without ferromagnetic shell.

Since the ring at the top of the iron-core will not enter the coil, and the push rod is made of carburized non-magnetic stainless steel, the impact on the magnetic field is small and can be ignored, the iron-core can be regarded as a standard cylinder for magnetic field analysis.

The modeling of the solenoid actuator magnetic field subdomain method assumes that the magnetic permeability of the iron-core is infinite, that is, the magnetic field lines on the iron-core are all perpendicular to the surface of the iron-core. In the calculation, the tangential component of the magnetic field is set at its boundary as zero. Magnetic field subdomain method modeling of solenoid actuator and setting of boundary conditions are shown in Figure 2.

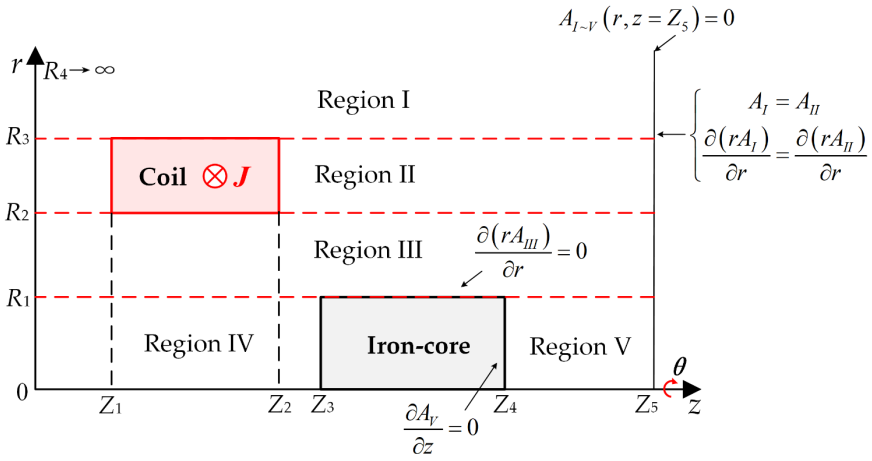

Figure 2. Magnetic field subdomain method modeling of a solenoid actuator and setting of boundary conditions.

Since the solenoid actuator is cylindrical, the magnetic field has axial symmetry characteristics, it is suitable to use the magnetic vector potential equation in cylindrical coordinates to solve. Take the central axis of the iron-core as the Z-axis and the radial direction as the R-axis. The entire solution domain is limited to three outer boundaries $(r, z = 0)$, $(r \to \infty, z)$ and $(r, z = Z_5)$. For more accurate solution results, each outer boundary should be kept away from the coil and the movement area of the iron-core.

According to Maxwell's equations and considering the Coulomb gauge, the relationship between the magnetic induction $\boldsymbol{B}$ and the magnetic vector potential $\boldsymbol{A}$ is derived from $\nabla \cdot \boldsymbol{A} = 0$ as

$$-\nabla \times \boldsymbol{B} = \nabla^2 \boldsymbol{A} = -\mu_0 \boldsymbol{J} . \tag{1}$$

 doi:10.20944/preprints202404.1258.v1

The magnetic field of the solenoid has rotational symmetry, and the rotation of the magnetic induction intensity only has the θ component, the magnetic vector $\boldsymbol{A}$ has only the θ component, and its magnitude is related to the coordinates of r and z, as shown in (2). Then the magnetic vector $\boldsymbol{A}$ can be expressed as A_θ or $A(r,z)$.

$$(\nabla \times \boldsymbol{B})_\theta = \frac{\partial B_r}{\partial z} - \frac{\partial B_z}{\partial r}. \tag{2}$$

The three components of solenoid magnetic induction intensity in the cylindrical coordinate system are [18]

$$B_r(r,z) = -\frac{\partial A_\theta}{\partial z}, B_\theta = 0, B_z(r,z) = \frac{1}{r}\frac{\partial (rA_\theta)}{\partial r}. \tag{3}$$

Substituting (3) into (2), it is obtained that the magnitude and potential $\boldsymbol{A}$ of the solenoid actuator satisfy

$$\nabla^2 \boldsymbol{A} = \frac{\partial^2 A_\theta}{\partial r^2} + \frac{1}{r}\frac{\partial A_\theta}{\partial r} - \frac{A_\theta}{r^2} + \frac{\partial^2 A_\theta}{\partial z^2} = -\mu_0 J(r,z). \tag{4}$$

Where μ_0 is the permeability in air and J is the current density in the coil. Express the current density as a function $J(r,z)$ related to r, z in order to distinguish the air regions where the current density is zero, and then distinguish the application area of Poisson equation and Laplace equation.

Solve the homogeneous differential equation using the separation of variables method. Let $A_\theta(r,z) = R(r)Z(z)$ and substitute it into (4) and multiply both sides by $1/RZ$ to get

$$\frac{1}{Z}\frac{\partial^2 Z}{\partial z} - \frac{1}{r^2} + \frac{1}{r}\cdot\frac{1}{R}\frac{\partial R}{\partial r} + \frac{1}{R}\frac{\partial^2 R}{\partial r^2} = 0. \tag{5}$$

Assuming that $\frac{1}{Z}\frac{\partial^2 Z}{\partial z} = -\alpha^2$, its solution is $x = \alpha r$, substituting into (5) to get

$$\begin{cases} \dfrac{\partial^2 Z}{\partial z} + \alpha^2 Z = 0 \\ \dfrac{\partial^2 R}{\partial x^2} + \dfrac{1}{x}\dfrac{\partial R}{\partial x} - \left(1 + \dfrac{1}{x^2}\right)R = 0 \end{cases}. \tag{6}$$

From $Z(0) = 0$ and $Z(\infty) = 0$ can know that Z is not a mediocre solution and $\alpha^2 > 0$, the above formula of (6) is a second-order constant coefficient homogeneous differential equation, and the general solution satisfies

$$Z(z) = c_1 \cos(\alpha z) + c_2 \sin(\alpha z). \tag{7}$$

The following formula of (6) conforms to the form of a first-order imaginary Bessel function (also known as modified Bessel function), and its general solution is

$$R(x) = c_3 I_1(x) + c_4 K_1(x). \tag{8}$$

Where $c_1 \sim c_4$ are constants, I_1 represents the first-order modified Bessel function, and K_1 represents the first-order modified Hank function.

Substitute $x = \alpha r$ into (8) and $A_\theta(r,z) = R(r)Z(z)$ to get the general solution equation of the magnetic vector potential in the region I~V and then

$$A_\theta(r,z) = \sum_{n=1}^{\infty}\left[c_1 \cos(\alpha_n z) + c_2 \sin(\alpha_n z)\right]\left[c_3 I_1(\alpha_n r) + c_4 K_1(\alpha_n r)\right]. \tag{9}$$

 doi:10.20944/preprints202404.1258.v1

According to the convergence and divergence of the modified Bessel function and Hank function of the magnetic vector potential of the cylindrical coordinate system at the outer boundary of the magnetic field, the general solution form of the simplified magnetic vector potential of each subdomain can be obtained respectively.

$$\begin{cases} A_I(r,z)=\sum_{n=1}^{\infty} b_n^I K_1(a_n r)\sin(a_n z) \\ A_{II}(r,z)=\sum_{n=1}^{\infty}\left\{a_n^{II} I_1(a_n r)+b_n^{II} K_1(a_n r)-C_n L_1(a_n r)\right\}\sin(a_n z) \\ A_{III}(r,z)=\sum_{n=1}^{\infty}\left\{a_n^{III} I_1(a_n r)+b_n^{III} K_1(a_n r)\right\}\sin(a_n z) \\ A_{IV}(r,z)=\sum_{k=1}^{\infty} a_k^{IV} I_1(\beta_k r)\sin(\beta_k z) \\ A_V(r,z)=\sum_{k=1}^{\infty} a_k^{V} I_1(\lambda_k r)\cos\left(\lambda_k (z-Z_4)\right) \end{cases}, \tag{10}$$

where

$$C_n=\mu_0(\pi/2)J_n\alpha_n^{-2},\ J_n=\frac{2J}{n\pi}\left(\cos(\alpha_n Z_1)-\cos(\alpha_n Z_1)\right), \tag{11}$$

and n is a positive integer, k is a positive odd number, and μ_0 is the magnetic permeability of air, taking $4\pi\times10^{-7}$ H/m. Substitute the external boundary conditions into (10) to obtain $\alpha_n=n\pi/Z_5$, $\lambda_k=k\pi/\left(2(Z_5-Z_4)\right)$. I_0 is the zero order modified Bessel functions, K_0 is the zero order modified Hank functions, and L_0, L_1 are the zero and first order modified Struve functions. b_n^I, a_n^{II}, b_n^{II}, a_n^{III}, b_n^{III}, a_k^{IV} and a_k^V are the integral coefficients of each region, determined by the boundary conditions between different regions.

By further substituting the inter-domain boundary conditions into (10) to obtain

$$a_n^{II}=\alpha_n R_3 C_n\left(L_0(\alpha_n R_3)K_1(\alpha_n R_3)+L_1(\alpha_n R_3)K_0(\alpha_n R_3)\right), \tag{12}$$

$$b_n^{II}=b_n^I+\alpha_n R_3 C_n\left(L_1(\alpha_n R_3)I_0(\alpha_n R_3)-L_0(\alpha_n R_3)I_1(\alpha_n R_3)\right), \tag{13}$$

$$a_n^{III}=a_n^{II}-\alpha_n R_2 C_n\left(L_1(\alpha_n R_2)K_0(\alpha_n R_2)+L_0(\alpha_n R_2)K_1(\alpha_n R_2)\right), \tag{14}$$

$$b_n^{III}=b_n^{II}+\alpha_n R_2 C_n\left(L_0(\alpha_n R_2)I_0(\alpha_n R_2)-L_1(\alpha_n R_2)I_0(\alpha_n R_2)\right), \tag{15}$$

$$a_n^{III}-b_n^{III}\frac{K_0(\alpha_n R_1)}{I_0(\alpha_n R_1)}=\sum_{k=1}^{\infty}\left(a_k^{IV}\frac{k}{nZ_3}\frac{I_0(\beta_k R_1)}{I_0(\alpha_n R_1)}f(n,k)+a_k^{V}\frac{k}{n(Z_5-Z_4)}\frac{I_0(\lambda_k R_1)}{I_0(\alpha_n R_1)}g(n,k)\right), \tag{16}$$

$$a_k^{IV}=\frac{2}{Z_3}\sum_{n=1}^{\infty}\left(a_n^{III}\frac{I_1(\alpha_n R_1)}{I_1(\beta_k R_1)}+b_n^{III}\frac{K_1(\alpha_n R_1)}{I_1(\beta_k R_1)}\right)\times f(n,k), \tag{17}$$

$$a_k^{V}=\frac{2}{Z_5-Z_4}\sum_{n=1}^{\infty}\left(a_n^{III}\frac{I_1(\alpha_n R_1)}{I_1(\lambda_k R_1)}+b_n^{III}\frac{K_1(\alpha_n R_1)}{I_1(\lambda_k R_1)}\right)\times g(n,k), \tag{18}$$

where

Preprints.org (www.preprints.org) | NOT PEER-REVIEWED | Posted: 18 April 2024 doi:10.20944/preprints202404.1258.v1

$$f(n,k)=\begin{cases}-\dfrac{\alpha_n \sin(k\pi/2)\cos(\alpha_n Z_3)}{(\alpha_n^2-\beta_k^2)} & for\ \alpha_n \neq \beta_k \\ 0.5\times Z_3 & for\ \alpha_n=\beta_k\end{cases}, \tag{19}$$

$$g(n,k)=\begin{cases}-\dfrac{\alpha_n \cos(\alpha_n Z_4)}{(\alpha_n^2-\lambda_k^2)} & for\ \alpha_n \neq \lambda_k \\ 0.5\times(Z_5-Z_4)\sin(\alpha_n Z_4) & for\ \alpha_n=\lambda_k\end{cases}. \tag{20}$$

When solving, first calculate a_n^{II} and a_n^{III} directly by (12) and (14), and then substitute a_n^{III} into (16), (17), and (18) and expand the sum series into matrix form to solve b_n^{III}, a_k^{IV} and a_k^{V}, and finally substituting b_n^{III} into (13) and (15) to obtain b_n^{I} and b_n^{II}. When all the coefficients are known, the magnetic vector potential $\boldsymbol{A}$ in the whole solution domain can be obtained by substituting into (10).

3.2. Inductance Equation Based on Subdomain Method

The inductive energy storage of the solenoid actuator is distributed in the conductive medium, and its total magnetic energy formula is

$$\frac{1}{2}L_m I^2=\frac{1}{2}\int_V A\cdot J dv. \tag{21}$$

Where L_m is the inductance value with iron-core, I is the current in the coil, and V is the volume of the conductor.

Assuming that the current in the coil is evenly distributed on the rectangular section of the coil, the current density value is equal to the current value divided by the area of the rectangular section, and the inductance value of the iron-core is

$$L_m=\frac{2\pi N^2}{(R_3-R_2)^2 L^2 J}\sum_{n=1}^{\infty}\left\{\frac{\pi}{2\alpha_n^2}\left(\begin{array}{c}a_n^{II}\left(R_3U(R_3)-R_2U(R_2)\right)\\ +b_n^{II}\left(R_3V(R_3)-R_2V(R_2)\right)\\ -C_n\dfrac{\alpha_n^3}{3\pi^2}\left(R_3^4W(R_3)-R_2^4W(R_2)\right)\end{array}\right)\cdot\left(\cos(\alpha_n Z_1)-\cos(\alpha_n Z_2)\right)\right\}, \tag{22}$$

where

$$\begin{cases}U(r)=I_1(\alpha_n r)L_0(\alpha_n r)-I_0(\alpha_n r)L_1(\alpha_n r)\\ V(r)=K_1(\alpha_n r)L_0(\alpha_n r)-K_0(\alpha_n r)L_1(\alpha_n r)\\ W(r)=F(1,2;3/2,5/2,3;\alpha_n^2 r^4/6\pi)\end{cases}. \tag{23}$$

and L is coil length, N is coil turns, and F represents Hypergeometric function.

From (22) can be seen that when the structural dimensions of the coil and the iron-core are known, as long as the instantaneous position of the movable iron-core and the current in the coil are known, the inductance value of the corresponding position can be obtained by the magnetic field subdomain method. In fact, when the *B-H* curve is not considered, the inductance value has nothing to do with the current, and the calculated inductance of the subdomain method also does not change with the current.

Preprints.org (www.preprints.org) | NOT PEER-REVIEWED | Posted: 18 April 2024 doi:10.20944/preprints202404.1258.v1

3.3. Electromagnetic Characteristics Analysis of the Push-Pull Electromagnet

In order to verify the accuracy of the inductance calculation, an ANSOFT Maxwell simulation model was built according to the structural parameters of the push-pull electromagnet in Figure 1, and wrote a MATLAB numerical calculation program. The parameters are shown in Table 1. When the relative position of the core to the center of the coil is 17.3 mm, the comparison between the gradient plot of magnetic vector potential calculated by the subdomain method and the FEM is shown in Figure 3.

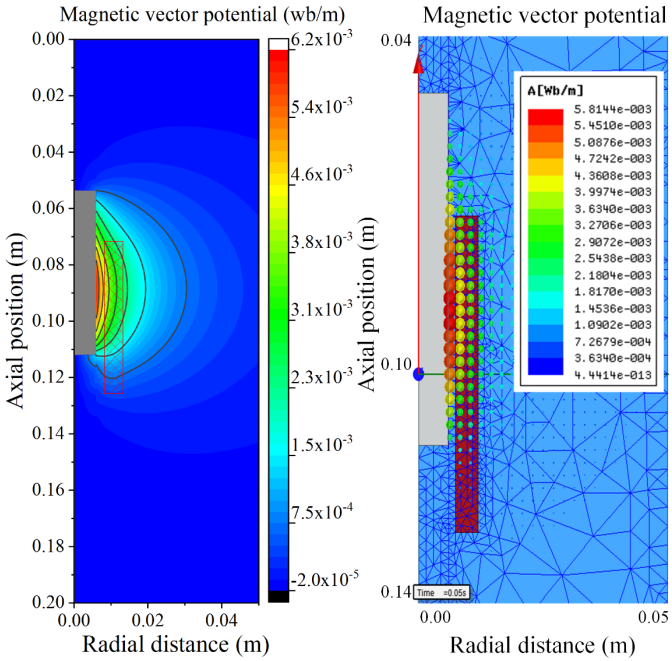

Figure 3. Comparison of magnetic vector potential calculated by subdomain method and FEM. Left: Calculated by subdomain method based on MATLAB programming; Right: Simulated by ANSOFT Maxwell.

Table 1. Analysis parameters of an electromagnetic actuator.

Symbol	Quantity	Value
R_1	Radius of the iron	5.9 mm
R_2	Inner Radius of the coil	7.4 mm
R_3	Outer Radius of the coil	12.0 mm
R_4	Radial boundary of the solution domain	50.0 mm
L	Axial length of the coil	52 mm
l	Axial length of the iron-core	58 mm
h	Relative displacement of coil and armature center	variable
Z_1	Axial position of the coil (left side)	74 mm
Z_3	Axial position of the iron-core (left side)	53.7 mm
Z_5	Outer boundary of the coil	200 mm
N	Number of turns of the coil	720
I	Excitation current of the coil	7.24 A
N_{max}	Number of harmonic terms in Region III and III	40
K_{max}	Number of harmonic terms in Region IV and V	40

 doi:10.20944/preprints202404.1258.v1

The comparison of the inductance curves of the movable iron-core at different axial positions relative to the center of the coil is shown in Figure 4, and a data point is taken every 0.5 mm. Among them, the magnetic permeability of the iron-core in the finite element is calculated according to the constant value of 10000 and the *B-H* curve of electrical iron (DT4) [5].

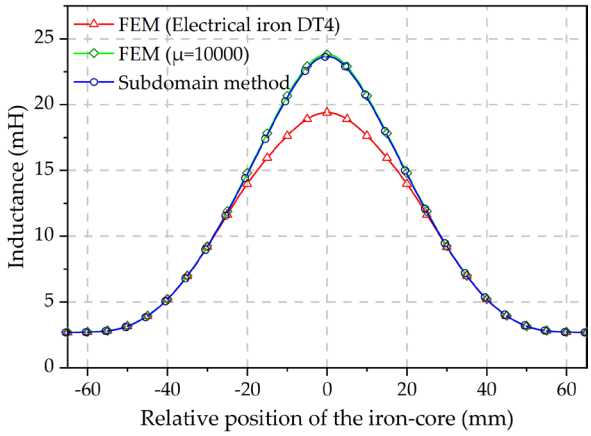

Figure 4. FEM and MATLAB programming calculated inductance comparison.

It can be seen from Figure 4 that the inductance calculated by the subdomain method is basically the same as the result when the relative magnetic permeability in the FEM is 10000, which shows that the calculation of subdomain method is accurate when the iron-core has high magnetic permeability and does not consider magnetic saturation. When the core is calculated according to the *B-H* curve of the electrical iron (DT4), the closer the relative position of the iron-core and the coil is, the greater the difference in the calculated inductance, which means that when the iron-core and the coil are in these relative positions, the 7.24 A current excitation has caused the magnetic core to occur a slight magnetic saturation.

After the inductance curve is obtained, the EMF on the iron-core can be calculated through the change of the inductance gradient. Use the virtual displacement method to solve the kinematic process. The EM energy of the system is [14]

$$W = \frac{1}{2} L(x) \cdot i^2(t) \tag{24}$$

Where W is the magnetic induction energy, $L(x)$ is the inductance value related to the position of the movable iron-core, $i(t)$ is the excitation current of the coil, and the EMF that the iron-core receives in the axial direction of the coil is [15]

$$F_{mag} = \frac{\mathrm{d}W}{\mathrm{d}x} = \frac{1}{2} i^2(t) \cdot \frac{\partial L(x)}{\partial x} \tag{25}$$

The EMF comparison of the movable iron-core at different axial positions relative to the coil is shown in Figure 5. As can be seen that the calculated EMF curve is wavy, this conforms to the property of the sum function of harmonic order of magnetic vector.

 doi:10.20944/preprints202404.1258.v1

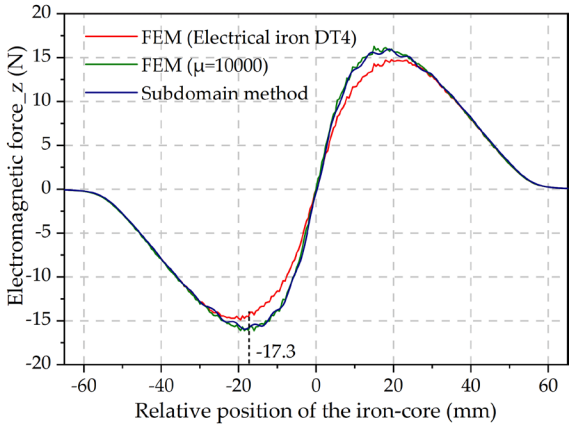

Figure 5. FEM and MATLAB programming calculated electromagnetic force comparison.

3. Experimental Platform Construction and Algorithm Verification

3.1. Verification of the Calculated Electromagnetic Force

In order to verify the accuracy of the magnetic field subdomain method to calculate the EMF of the solenoid actuator, an EMF test experimental platform was built. In this stage of the experiment, the spring was disassembled and the influence of the spring force was eliminated.

For accurate analysis, the experimental platform in this study is arranged longitudinally, which can reduce the errors caused by the friction force and the eccentricity of the magnetic core. Use the stepper motor lifting platform to adjust the iron-core to move down by 8.2 mm. In order to avoid errors caused by the force sensor's own gravity and installation preload on the test results, the transmitter should be zeroed before the test. This operation also eliminates the gravity of the iron-core.

The experimental platform for testing the EMF is shown in Figure 6. Apply 12 VDC to the coil, the current data detected by the current sensor and the EMF data detected by the force sensor are shown in Figure 7.

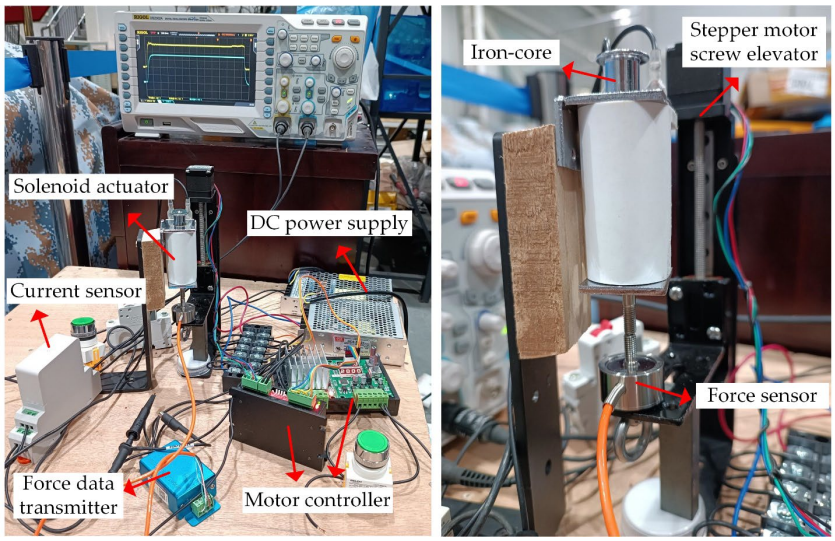

Figure 6. Electromagnetic force test platform of the push-pull electromagnet.

 doi:10.20944/preprints202404.1258.v1

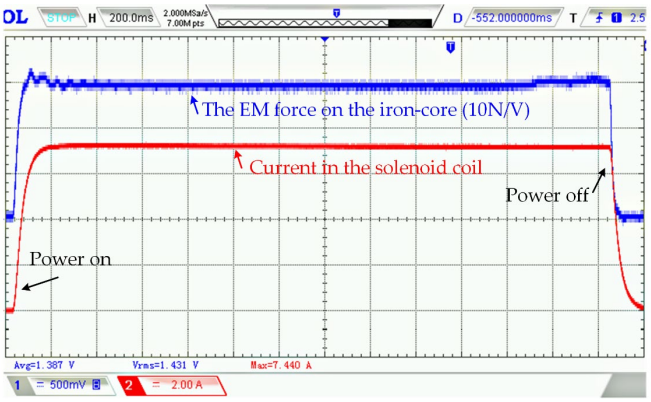

Figure 7. Oscilloscope display in the electromagnetic force test.

In the experiment, the average current after stabilization is 7.239 A, the average EMF after stabilization is 14.704 N, the EMF calculated by the subdomain method is 15.75 N, and the FEM result using electrical iron (DT4) is 14.33 N. If the EMF measured in the experiment is used as the benchmark, the calculation accuracy of the FEM and the subdomain method are 97.46 % and 92.89 %, respectively.

The semi-analytical method has the advantage of flexible calculation. It can calculate the dynamic EMF according to the changing current, which is helpful to study the EMF dynamic response characteristics of the solenoid actuator. The varying current can be measured by a sensor or calculated by a circuit with a resistive inductive load. The comparison between the EMF calculated according to the tested current and the EMF directly tested by the force sensor in the experiment is shown in Figure 8.

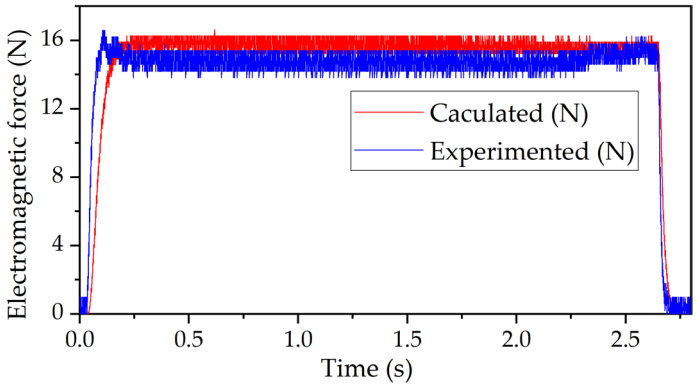

Figure 8. Comparison of the calculated electromagnetic force and the experimental data.

As shown in Figure 8, since the experimental platform is suddenly vibrated by EMF, the force curve of the test will have a stable process. In the calculation, it is assumed that the iron-core is completely fixed, of course the inductance gradient will not change due to the vibration of the experimental platform, therefore the calculated EMF does not have a stable process.

3.2. Verification of the Calculated Output Thrust

The above analysis shows the accuracy of the subdomain method for calculating the EMF, but in practical applications, the output thrust of the push-pull electromagnet is the most concerned by the users, so the force of the spring and the gravity of the iron-core must be considered. Compared with the FEM, the semi-analytical method can better deal with these factors that affect the output thrust and realize the calculation.

In order to verify the accuracy of the output thrust calculation, a mechanical analysis and output thrust test platform was conducted as shown in Figure 10.

 doi:10.20944/preprints202404.1258.v1

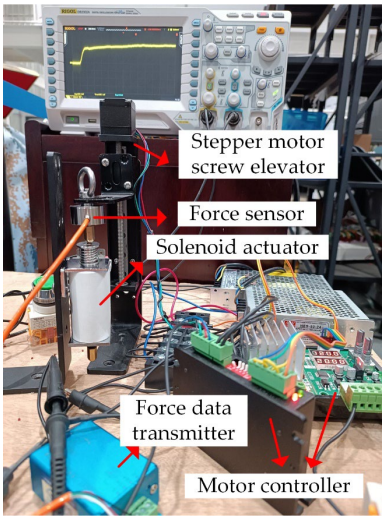

Figure 9. Spring force test experiment.

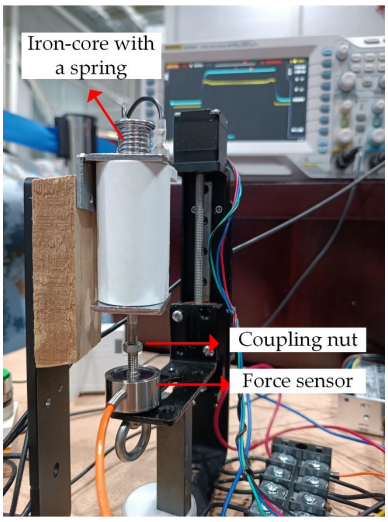

Figure 10. Output thrust test experiment.

The force sensor transmitter is zeroed and then connected with the iron-core using a connecting nut. At this time, if the solenoid is energized, the force measured by the force sensor is a resultant of the spring force, the core gravity, and the EMF, which is also the output thrust when the push-pull electromagnet is arranged longitudinally. Taking the downward direction as the positive direction, the output thrust is expressed as

$$F_t = F_{mag} + M + F_s \tag{26}$$

Where M is the gravity of the iron-core, $F_s = -kx$ is the spring force, x is the compression of the spring, and k is the force coefficient of the spring.

Since the force coefficient k of the tested spring is unknown, it is necessary to obtain the force of the spring at different degrees of compression through experiment. The spring force test experimental platform is shown in Figure 9. During the test, the coil is not energized. The stepper motor lifting platform is moved down at a constant speed and the pressure sensor compresses the spring at a constant speed. During this test process, the force detected by the sensor is $(M - kx)$, which is already considered the gravity of the iron-core. The force sensor detects the spring force waveform corresponding to different compression amounts (the data is Savitzky-Golay smoothed [19]) as shown in Figure 11.

Preprints.org (www.preprints.org) | NOT PEER-REVIEWED | Posted: 18 April 2024 doi:10.20944/preprints202404.1258.v1

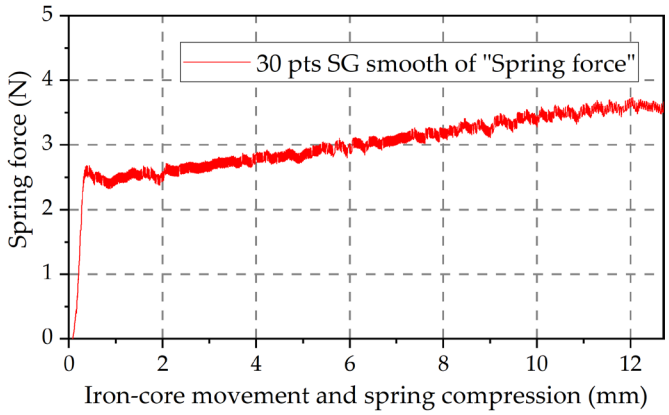

Figure 11. Relation between spring force and compression.

The working stroke of the push-pull electromagnet used in the experiment is 12.7 mm, and the relative position of the movable iron-core and coil is −25.5 mm~−12.8 mm, take the EMF of the corresponding interval in Figure 5 for calculation, the output thrust of the iron-core is the EMF minus the spring force. The calculation results are shown in Figure 12.

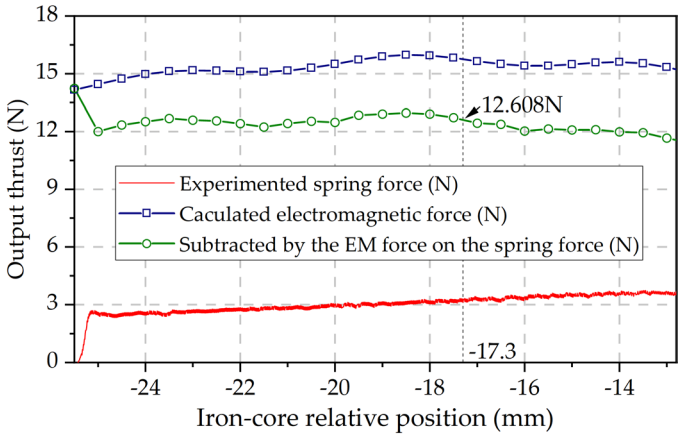

Figure 12. Output thrust calculation of the push-pull electromagnet in the stroke range.

It can be seen from Figure 12 that when the push rod is compressed by 8.2 mm, the calculated theoretical output thrust of the push-pull electromagnet should be 12.608 N. The current and thrust waveform displayed by the oscilloscope in the experiment are shown in Figure 13.

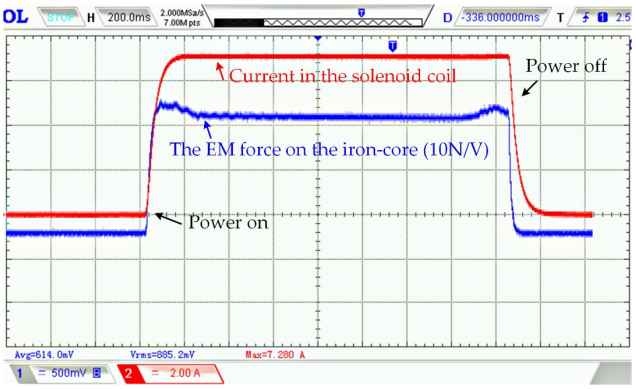

Figure 13. Oscilloscope display in the output thrust test experiment.

 doi:10.20944/preprints202404.1258.v1

Due to the spring force, the force sensor detects the upward pulling force before the solenoid is energized, and when we set the sensor to output positive data when under pressure, the pulling force is correctly displayed as a negative value. The total output EMF tested in the experiment is 11.23 N, and the calculation accuracy of the magnetic subdomain method is 87.29 % as a comparison.

5. Conclusions

Solenoid actuator is a typical EM energy and mechanical energy conversion device. Although it has been widely used in many industrial applications, the magnetic field calculation of solenoids with movable iron-cores has always been a difficult research point. The calculation at this stage is basically handled by finite element, and there are many drawbacks. In this study, the EM characteristic data of solenoid actuator is calculated accurately by the magnetic field subdomain method. When the excitation current applied to the coil is 7.24 A, the accuracy of calculating the EMF is 92.89%.

Compared with the FEM, the magnetic field subdomain method has the advantages of programmable and flexible calculation. Using these advantages, many calculations that cannot be processed by the FEM can be realized, such as the construction of intelligent algorithms such as genetic algorithms to optimize the design parameters of EM actuators. In this study, the calculation of the iron-core output thrust of a push-pull EM actuator without a ferromagnetic shell is realized by MATLAB programming, and the calculation accuracy is 87.29%. The disadvantage is that the magnetic permeability of the iron-core is regarded as infinite in the calculation process, and the influence of the eddy current on the surface of the iron-core is ignored, and the calculation accuracy will be reduced in the case of high current strong magnetic field or low magnetic permeability iron-core.

Author Contributions: Conceptualization, methodology, software, and validation, M.L.; formal analysis, investigation, resources, and data curation, X.Y.; writing—original draft preparation and writing—review and editing, M.L.; project administration and funding acquisition, Z.Y. All authors have read and agreed to the published version of the manuscript.

Funding: This work was supported in part by the General Surface Program of Natural Science Foundation of Hubei Province No. 506.

Data Availability Statement: The original contributions presented in the study are included in the article material, further inquiries can be directed to the corresponding author.

Acknowledgments: The authors would like to thank the editors and anonymous reviewers for their valuable comments and suggestions.

Conflicts of Interest: The authors declare no conflicts of interest.

References

1. Afshar, S.; Khamesee, M.B.; Khajepour, A. Optimal configuration for electromagnets and coils in magnetic actuators. *IEEE Trans. Magn.* **2012,** 49, 1372-1381.
2. Hassannia, A.; Abedi, K. Optimal switching scheme for multistage reluctance coilgun. *IEEE Trans. Plasma Sci.* **2021**, 49, 1241-1246.
3. Lu, M.; Zhang, J.; Yi, X.; Zhuang, Z. Advanced mathematical calculation model of single-stage RCG. *IEEE Tran. Plasma Sci.* **2022**, 50, 1026-1031.
4. Lequesne, B. Automotive electrification: The nonhybrid story. *IEEE Trans. Transp. Electr.* **2015**, 1, 40-53.
5. Wu, S.; Zhao, X.; Li, C.; Jiao, Z.; Qu, F. Multiobjective optimization of a hollow plunger type solenoid for high speed on/off valve. *IEEE Trans. Ind. Electron.* **2017**, 65, 3115-3124.
6. Li, K.; Luo, C.; Niu, F.; Li, C.; Tong, M.; Wu, Y. A new magnetic release design with high anti-interference capability. *IEEE Trans. Magn.* **2021**, 57, 1-9.
7. Cao, Z.; Zuo, Y. Electromagnetic riveting technique and its applications. *Chinese J. Aeronaut.* **2020**, 33, 5-15.
8. Hogan, P.H.; Van de Ven, J.D. Dynamic modeling of a linear electromagnetic piston pump. in *Proc. ASME/BATH 2017 Symp. Fluid Power Motion Control Amer. Soc. Mech. Eng.*, **2017**, V001T01A062.
9. Barbetta, M.; Boesso, A.; Branz, F.; Carron, A.; Olivieri, L.; Prendin, J.; Francesconi, A. ARCADE-R2 experiment on board BEXUS 17 stratospheric balloon. *CEAS Space J.* **2015**, 7, 347-358.

 doi:10.20944/preprints202404.1258.v1

10. Goeller, M.; Oberlaender, J.; Uhl, K.; Roennau, A., Dillmann, R. Modular robots for on-orbit satellite servicing. In *IEEE international conference on robotics and biomimetics* (ROBIO), **2012**, 2018-2023.
11. Song, C.W.; Lee, S.Y. Design of a solenoid actuator with a magnetic plunger for miniaturized segment robots. *Applied sciences* **2015**, 5, 595-607.
12. Alizadeh, H.V.; Boulet, B. Analytical calculation of the magnetic vector potential of an axisymmetric solenoid in the presence of iron parts. *IEEE Trans. Magn.* **2015**, 52, 1-4.
13. Liang, P.; Chai, F.; Bi, Y.; Pei, Y.; Cheng, S. Analytical model and design of spoke-type permanent-magnet machines accounting for saturation and nonlinearity of magnetic bridges. *J. Magn. Magn. Mater.* **2016**, 417, 389-396.
14. Lubin, T.; Berger, K.; Rezzoug, A. Inductance and force calculation for axisymmetric coil systems including an iron core of finite length. *Progress In Electromagnetics Research B* **2012**, 41, 377-396.
15. Elbaa, M.K.; Berger, B.; Douine, M. Halit, Bentridi S.E. Analytical modeling of an inductor in a magnetic circuit for pulsed field magnetization of HTS bulks. *IEEE Trans. Appl. Supercon.* **2018**, 28, 1-6.
16. Luo, Y. Field and inductance calculations for coaxial circular coils with magnetic cores of finite length and constant permeability. *IET Electr. Power App.* **2017**, 11, 1254-1264.
17. Jebelli, A.; Mahabadi, A.; Yagoub, M.C.; Chaoui, H. Magnetic force calculation between magnets and coil. *International Journal of Physics* **2020**, 8, 71-80.
18. Pankrac,V.; Kracek, J. Simple algorithms for the calculation of the intensity of the magnetic field of current loops and thin-wall air coils of a general shape using magnetic dipoles. *IEEE Trans. Magn.* **2012**, 48, 4767-4778.
19. Kojooyan-Jafari, H.; Monjo, L.; Córcoles, F.; Pedra J. Parameter estimation of wound-rotor induction motors from transient measurements. *IEEE Trans. Energy Conver.* **2014**, 29, 300-308.